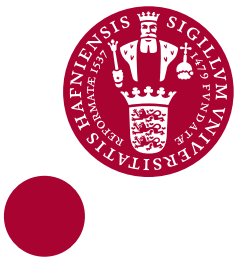

Loss of PICH Results in Chromosomal Instability, p53 Activation, and Embryonic Lethality

Albers, Eliene; Sbroggiò, Mauro; Pladevall-Morera, David; Bizard, Anna H.; Avram, Alexandra; Gonzalez, Patricia; Martin-Gonzalez, Javier; Hickson, Ian D.; Lopez-Contreras, Andres J.

Published in:
Cell Reports

DOI:
10.1016/j.celrep.2018.08.071

Publication date:
2018

Document version
Publisher's PDF, also known as Version of record

Cell Reports

Article

Loss of PICH Results in Chromosomal Instability, p53 Activation, and Embryonic Lethality

Graphical Abstract

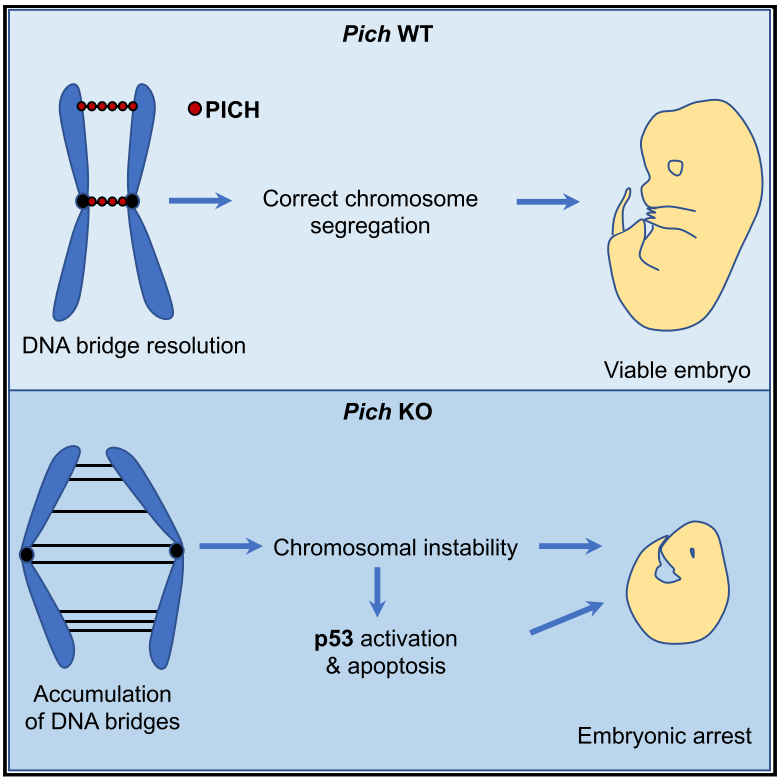

Authors

Eliene Albers, Mauro Sbroggiò, David Pladevall-Morera, ..., Javier Martin-Gonzalez, Ian D. Hickson, Andres J. Lopez-Contreras

Correspondence

ajlopez@sund.ku.dk

In Brief

Albers et al. show that PICH is essential for mouse embryonic development and that PICH deficiency limits oncogenic-induced cellular transformation. These findings suggest that PICH activity is critical during events requiring rapid cell proliferation such as embryonic development and tumorigenesis.

Highlights

- *Pich* is essential for embryonic development
- *Pich* KO embryos exhibit DNA damage, p53 activation, and apoptosis
- *Pich* heterozygous mice are born at sub-Mendelian ratios
- *Pich*-deficient MEF are resistant to RAS^{V12}/E1A-induced transformation

Albers et al., 2018, Cell Reports *24*, 3274–3284
September 18, 2018
https://doi.org/10.1016/j.celrep.2018.08.071

CellPress

OPEN ACCESS
CellPress

Cell Reports
Article

Loss of PICH Results in Chromosomal Instability, p53 Activation, and Embryonic Lethality

Eliene Albers,[1,4] Mauro Sbroggiò,[1,4] David Pladevall-Morera,[1] Anna H. Bizard,[1] Alexandra Avram,[1] Patricia Gonzalez,[2] Javier Martin-Gonzalez,[3] Ian D. Hickson,[1] and Andres J. Lopez-Contreras[1,5,*]

[1]Department of Cellular and Molecular Medicine, Center for Chromosome Stability and Center for Healthy Aging, University of Copenhagen, Copenhagen 2200, Denmark

[2]Histopathology Core Unit, Spanish National Cancer Research Centre, Madrid 28029, Spain

[3]Transgenic Core Facility, Department of Experimental Medicine, University of Copenhagen, Copenhagen 2200, Denmark

[4]These authors contributed equally

[5]Lead Contact

*Correspondence: ajlopez@sund.ku.dk

https://doi.org/10.1016/j.celrep.2018.08.071

SUMMARY

PICH is a DNA translocase necessary for the resolution of ultrafine anaphase DNA bridges and to ensure the fidelity of chromosomal segregation. Here, we report the generation of an animal model deficient for PICH that allowed us to investigate its physiological relevance. *Pich* KO mice lose viability during embryonic development due to a global accumulation of DNA damage. However, despite the presence of chromosomal instability, extensive p53 activation, and increased apoptosis throughout the embryo, *Pich* KO embryos survive until day 12.5 of embryonic development. The absence of p53 failed to improve the viability of the *Pich* KO embryos, suggesting that the observed developmental defects are not solely due to p53-induced apoptosis. Moreover, *Pich*-deficient mouse embryonic fibroblasts exhibit chromosomal instability and are resistant to RAS^{V12}/E1A-induced transformation. Overall, our data indicate that PICH is essential to preserve chromosomal integrity in rapidly proliferating cells and is therefore critical during embryonic development and tumorigenesis.

INTRODUCTION

Chromosomal stability is challenged each time a cell undergoes DNA replication and segregates its genetic material to the daughter cells. Many factors have evolved to safeguard genomic integrity during these processes and to promote the fidelity of chromosome transmission. The resolution of interlinked sister chromatids (e.g., due to unfinished DNA replication, DNA repair intermediates, DNA catenation) that persist from S phase must occur before or during the anaphase of mitosis for successful sister chromatid disjunction to occur (Mankouri et al., 2013). In rare cases, these sister chromatid entanglements may persist until late anaphase, whereupon they require several factors for their resolution. Among these factors is PICH (PLK1-interacting checkpoint helicase), which, despite its importance in mitosis, is poorly characterized. PICH, also known as ERCC6L, was discovered as a PLK1 interacting protein (Baumann et al., 2007). Based on its protein sequence and the results of small interfering RNA (siRNA)-mediated depletion experiments, PICH was initially defined as a DNA helicase and mitotic checkpoint protein (Baumann et al., 2007). However, subsequent studies revealed that PICH lacks helicase activity and does not regulate the spindle assembly checkpoint (Hübner et al., 2010). Instead, PICH has double-stranded DNA (dsDNA) translocase activity and binds preferentially to DNA under tension *in vitro* (Biebricher et al., 2013).

PICH has an unusual pattern of subcellular localization. It localizes in the cytosol during interphase and is recruited to chromatin after nuclear envelope breakdown in prometaphase. During anaphase, PICH decorates so-called ultrafine anaphase DNA bridges (UFBs) (Baumann et al., 2007; Chan et al., 2007). UFBs cannot be detected with DNA dyes such as DAPI and lack histones, but they are generally defined by the presence of PICH along much or all of their length (Baumann et al., 2007; Chan et al., 2007). These mitotic DNA bridges can be found in most cells and are thought to consist of unresolved DNA replication intermediates and DNA catenanes that link the separating sister chromatids. UFBs usually arise from repetitive sequences such as telomeres, rDNA, and centromeres, or from common fragile sites (CFSs) (Nielsen and Hickson, 2016). PICH contributes to the resolution of UFBs, most likely by stimulating the catalytic activity of the TOP2a topoisomerase (Nielsen et al., 2015; Rouzeau et al., 2012). As a consequence, the lack of PICH leads to DNA segregation defects that result in the formation of micronuclei and aneuploidy (Hengeveld et al., 2015; Nielsen et al., 2015). Nevertheless, PICH is not essential for the viability of chicken DT40 or human cancer cell lines, although in both cases its depletion causes extensive genomic instability (Hengeveld et al., 2015; Nielsen et al., 2015).

Given the mitotic segregation defects observed in PICH-deficient cells, it is likely that PICH deficiency would have detrimental consequences *in vivo*; however, to date, there are no reports of animal models lacking functional PICH. Here, we have generated

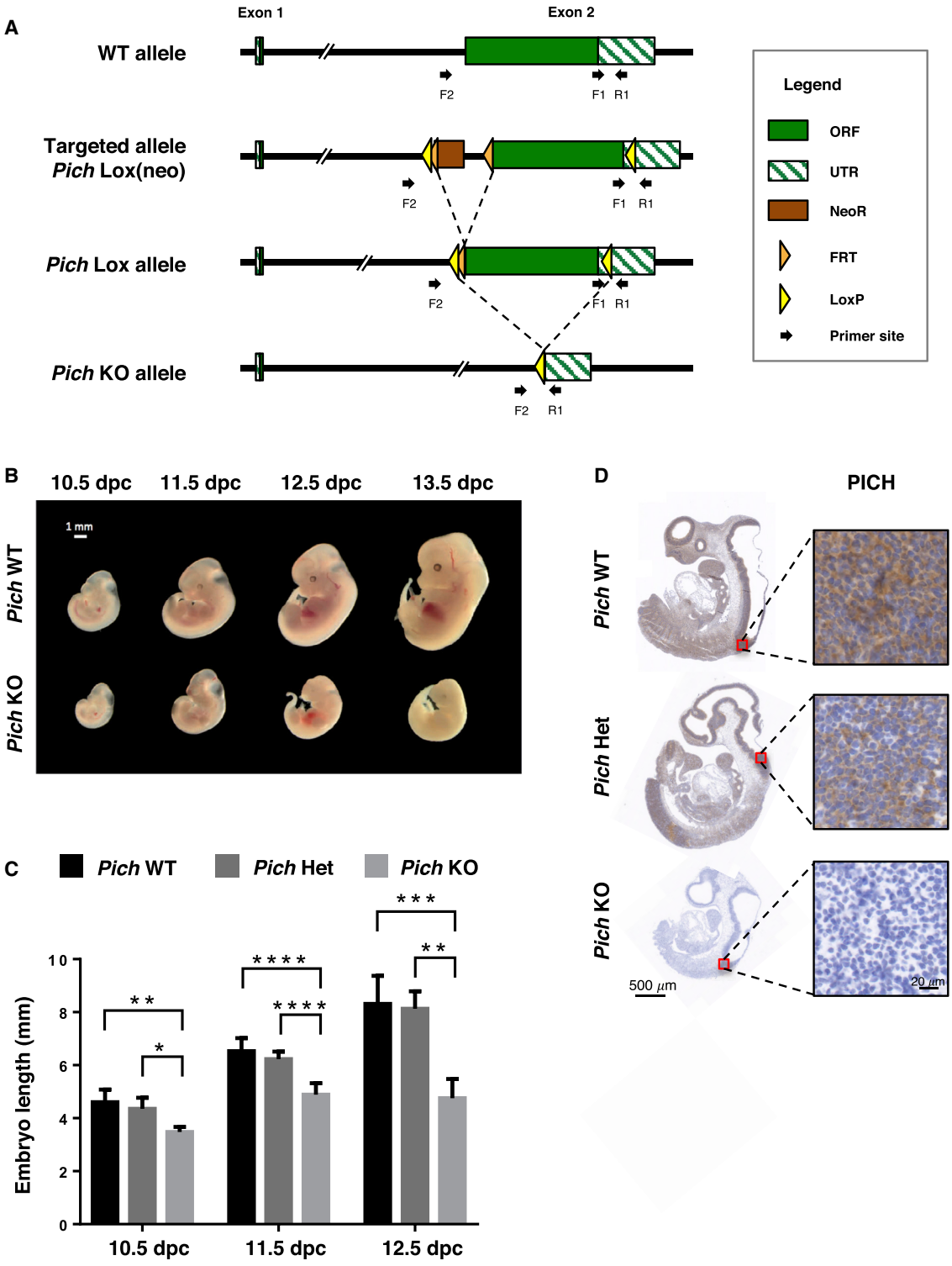

Figure 1. *Pich* KO Leads to Embryonic Lethality in Mice

(A) Gene-targeting strategy for the generation of *Pich* KO mice (see Experimental Procedures for details). ORF, open reading frame.

(B) Morphology of WT and *Pich* KO embryos at 10.5–13.5 days post-coitum (DPC). *Pich* KO embryos are smaller than WT embryos and die at approximately 12.5 DPC.

(legend continued on next page)

Table 1. Genotypes of Progeny from *Pich*$^{+/-}$ × WT Crosses

	Male Mice		Female Mice	
	Pich^{+}	*Pich*$^{-}$	*Pich*$^{+/+}$	*Pich*$^{+/-}$
Observed	24	0	132	84
Expected	12[a]	12[a]	108	108

[a]We stopped genotyping males from this strain after finding that Pich KO males were not born, while we continued genotyping more females.

a *Pich* knockout (KO) mouse model to investigate the relevance of PICH at the organismal level in mammals. Our results show that PICH is essential for embryonic development. *Pich* KO embryos and *Pich* KO mouse embryonic fibroblasts (MEFs) show high levels of genomic instability, which is incompatible with a sustained viability.

RESULTS

Generation of a *Pich* Conditional KO Mouse Model

The mouse *Pich* gene is located on the X chromosome and consists of two exons: a short exon 1 (204 bp) and a long exon 2 (4,039 bp) that encodes most of the protein. To study the consequences of PICH deficiency *in vivo*, we generated a conditional *Pich* KO mouse model in which the deletion of the *Pich* gene could be induced by the expression of Cre recombinase. We targeted this locus in mouse embryonic stem cells (mESCs) using a standard recombination strategy with a targeting construct containing a neomycin cassette for selection and two long homology arms for efficient recombination. We targeted exon 2 to ensure that most of the PICH protein-coding region would be excised upon Lox recombination (Figure 1A). Due to the large size of exon 2, inserting the LoxP sites in such a way as to flank the entire length of the exon would compromise the efficiency of Cre-mediated recombination. Therefore, one LoxP site was positioned inside the 3′ UTR of exon 2 (Figure 1A). Using this strategy, we successfully generated *Pich* conditional KO (*Pich*^{Lox}) mESC (Figures S1A and S1B). Following that, we generated male chimeras by microinjecting *Pich*^{Lox} mESC into WT embryos that were able to transmit the *Pich*^{Lox} allele to their progeny. *Pich*^{Lox} males and *Pich*$^{+/Lox}$ and *Pich*$^{Lox/Lox}$ females were born at expected Mendelian ratios and did not show any obvious phenotypic abnormalities.

Pich KO Mice Die during Embryonic Development

After removal of the neomycin cassette via a cross with *Flippase* mice, *Pich*$^{+/Lox}$ females were crossed with *UQ-CMV-Cre* transgenic males to generate mice harboring a *Pich* KO allele. Like *Pich*, the *UQ-CMV-Cre* allele is located on the X chromosome and was therefore transmitted only to females. The deletion of the Lox-targeted locus was efficient, and *Pich* heterozygous (Het) females were obtained. To generate *Pich* KO mice, *Pich* Het females were crossed with wild-type (WT) males. A total of 50% of the male offspring from this breeding would be expected to be *Pich* KOs. However, all of the males born were found to be WT for *Pich* (Table 1), indicating that PICH is essential for embryonic development. More important, *Pich* Het females were born, indicating that the Pich KO gene is transmitted to the offspring. However, *Pich* Het females were born at sub-Mendelian ratios; 40% of the females were *Pich* Het, whereas 60% were WT (Table 1).

To characterize the phenotype of the targeted mice, we examined embryos obtained from *Pich* Het females crossed with WT males at different developmental stages. *Pich* KO male embryos were obtained at 10.5, 11.5, 12.5, and 13.5 days post-coitum (DPC), although at a lower proportion than expected (Table 2). These results indicate that most *Pich* KO embryos lose viability at or before 13.5 days of embryonic development. It should be noted that *Pich* Het female embryos were observed at expected Mendelian ratios (Table 2). Next, we examined the morphology of *Pich* KO embryos. Although *Pich* KO embryos exhibited normal gross morphology at 10.5 DPC, they were smaller than their WT or *Pich* Het counterparts (Figures 1B and 1C). This difference in size became more evident after 11.5 DPC. We did not observe any obvious tissue-specific alteration, but rather a general developmental arrest incompatible with viability, which was particularly evident in the few *Pich* KO embryos found at 12.5 and 13.5 DPC (Figure 1B). At these stages *Pich* Het embryos were indistinguishable from WT littermates in terms of size and morphology.

We confirmed the absence of PICH protein in *Pich* KO embryos by immunohistochemistry (IHC) (Figure 1D). PICH is located in the cytosol of cells in interphase, and its presence on chromatin is restricted to mitosis. As expected, PICH IHC revealed a predominantly cytosolic pattern of PICH localization in interphase cells. In WT and Het embryos, PICH was detected in most embryonic tissues (Figures 1D, S1D, S2A, and S3A).

Pich KO Embryos Show a Global Increase in DNA Damage and Apoptosis

To characterize the phenotype of the *Pich* KO embryos, we performed IHC analysis for factors involved in genome stabilization or DNA damage signaling. Because PICH promotes accurate chromosome segregation, we examined whether the loss of PICH led to chromosomal instability. We detected an increase in the proportion of cells that are positive for γH2AX, a marker of DNA damage, in 10.5 DPC *Pich* KO embryos (Figures 2A, 2D, and S1E). Evidence of DNA damage was detectable in all of the tissues in the *Pich* KO embryos, but it was particularly evident in some areas, including the embryonic brain. Next, we assessed whether activation of the DNA damage response in *Pich* KO embryos could also lead to p53 stabilization. We observed a high number of p53 positive cells in *Pich* KO embryos at day 10.5 DPC and onward (Figures 2B, 2D, S1F, and S2C). Moreover, we observed an increase in the number of apoptotic cells in *Pich* KO embryos, as determined by IHC staining for

(C) Quantification of embryo length. Error bars indicate SD; data from at least three embryos per genotype.
(D) Immunohistochemical staining for PICH in WT, *Pich* heterozygous (Het), and *Pich* KO embryos at 10.5 DPC confirms the absence of PICH protein in *Pich* KO embryos.
*p < 0.05, **p < 0.01, ***p < 0.001, ****p < 0.0001. See also Figure S1.

Table 2. Genotypes of Embryos from Crosses between *Pich*$^{+/-}$ Females and WT Males

	Male Embryos		Female Embryos	
DPC	*Pich*$^{+}$	*Pich*$^{-}$	*Pich*$^{+/+}$	*Pich*$^{+/-}$
10.5	14	6	16	15
11.5	12	9	20	21
12.5	10	4	9	11
13.5	10	2	5	10

cleaved caspase-3 (Figures 2C, 2D, S1G, S2D, and S3D). These data indicate that the lack of PICH gives rise to DNA damage and p53 activation throughout the whole embryo, which ultimately leads to increased apoptosis and failure of the embryo to successfully complete development.

Pich KO MEF Exhibit Mitotic Defects and Impaired Proliferative Capacity

To further characterize the cause of embryonic lethality in the *Pich* KO mice, we generated MEFs from WT and *Pich* KO embryos at 10.5 and 11.5 DPC. We confirmed the absence of PICH expression in the KO MEFs by western blotting (Figure 3A). *Pich* KO MEFs proliferated at a lower rate than their WT counterparts (Figures 3B, S4A, and S4B) and entered into a senescent state after only three to four passages in culture, as determined by senescence-associated beta-galactosidase staining (Figures 3C and 3D). At early passages, *Pich* KO MEF incorporated 5-ethynyl-2′-deoxyuridine (EdU) poorly, indicating a very limited replicative capacity, and also showed a greater tendency to accumulate in the G2 cell-cycle phase as compared to WT cells (Figures 3E and 3F). The loss of PICH resulted in various phenotypes associated with genome instability, including increased levels of 53BP1 nuclear foci (Figures 4A and 4B), micronucleus formation (Figures 4A, 4C, and S4C), and polyploidy (Figures 3E and 3F). These results confirm that PICH-deficient cells have chromosomal segregation defects that result in the activation of the DNA damage response (DDR) and a reduction in proliferative capacity.

Pich Heterozygous Females Are Born at Sub-Mendelian Ratios

As mentioned above, *Pich* Het females are born at sub-Mendelian proportions (Table 1). Of 216 females obtained, 132 were WT and 84 were *Pich* Het. Given that the proportion of *Pich* Het female embryos at 12.5 DPC was Mendelian (Table 2) and that we genotyped these mice at 4 weeks of age, ~20% of *Pich* Het females died either during the latter stages of embryonic development or perinatally. We believe that this lethality is most likely explained by the random X chromosome inactivation that affects the remaining *Pich* WT allele. *Pich* Het embryos showed a mosaic pattern of PICH expression that was compatible with random chromosome X inactivation (Figures 1D and S1D). However, we cannot rule out that the *Pich* gene escapes from full inactivation, as has been reported for *Pich* in mESCs (Marks et al., 2015), and low levels of PICH may still be expressed in all of the cells. The penetrance of the phenotype was variable, similar to human X-linked disorders. While ~20% of *Pich* Het females died, the rest were born and did not show any obvious abnormalities, as reflected in their similar appearance and weight as compared to WT littermates (Figures S4E and S4F). *Pich* Het females exhibited reduced fertility and they produced fewer pups (4.6 ± 2.3) than did WT females (15.8 ± 2.9) during a 14-week period (Figure S4G). Of note, two of the *Pich* Het females studied did not produce any viable pups (Figure S4G).

The *Pich* Het embryos analyzed at 10.5, 11.5, and 12.5 DPC were similar in size and morphology to their WT littermates (Figure 1C). *Pich* Het MEFs proliferated at a slightly lower rate than their WT counterparts (Figure 3B). *Pich* Het MEFs exhibited a mild but significant increase in the number of 53BP1 foci and micronuclei as compared to their WT counterparts (Figures 4B and 4C), indicative of genomic instability.

Loss of p53 Does Not Rescue *Pich* KO Embryonic Lethality

We observed increased p53 stabilization in *Pich* KO embryos (Figures 2B, S1F, S2C, and S3C). p53 stabilization leads to the induction of apoptosis and senescence (Haupt et al., 2003; Itahana et al., 2001), which could contribute to the embryonic lethality that is observed in *Pich* KO embryos. To investigate this possibility, we crossed our *Pich* KO model with *Trp53* KO mice (Jacks et al., 1994). The loss of p53 has been demonstrated to rescue the lethality of other mouse models with defective DNA repair, such as *Brca1*- and *DNA Ligase IV*-deficient mice (Frank et al., 2000; Xu et al., 2001). However, no viable *Pich* KO mice were born in the absence of *Trp53* or in a *Trp53* heterozygous background (Table 3). In addition, we did not observe a rescue in the phenotype of *Pich* KO embryos at 10.5 days of embryonic development in the absence of *Trp53* (Table S1; Figure S5). These data suggest that p53-dependent apoptosis and senescence are unlikely to be the sole drivers of *Pich* KO embryonic lethality.

To further characterize the interaction between these two genes, we derived WT and *Pich* KO mESCs from our mouse model. These cell lines were infected with retroviruses expressing either control small hairpin RNA (shRNA) or a previously validated *Trp53* shRNA (Murga et al., 2009) (Figure S6A). We could not perform these experiments in MEFs due to the reduced proliferative capacity of *Pich* KO MEFs. The number of cells with high levels of γH2AX or more than two 53BP1 foci per nucleus were increased in *Pich* KO mESCs as compared to WT mESCs. Both of these phenotypes were slightly increased upon knockdown of *Trp53* (Figures S6B and S6C).

In agreement with the above, rather than providing a rescue, our data indicate that the proportion of successful viable births in *Pich* Het females was further reduced in a *Trp53* null background; only one *Pich*$^{+/-}$;*Trp53*$^{-/-}$ female was born out of seven expected (Table 3). This observation suggests that a partial synthetic lethal interaction between these two genes may occur in a scenario with reduced levels of PICH.

In Silico Analysis of the Impact of PICH Status on Human Cancer

Given the relevance of PICH during embryonic development, we wanted to address the potential impact of PICH in

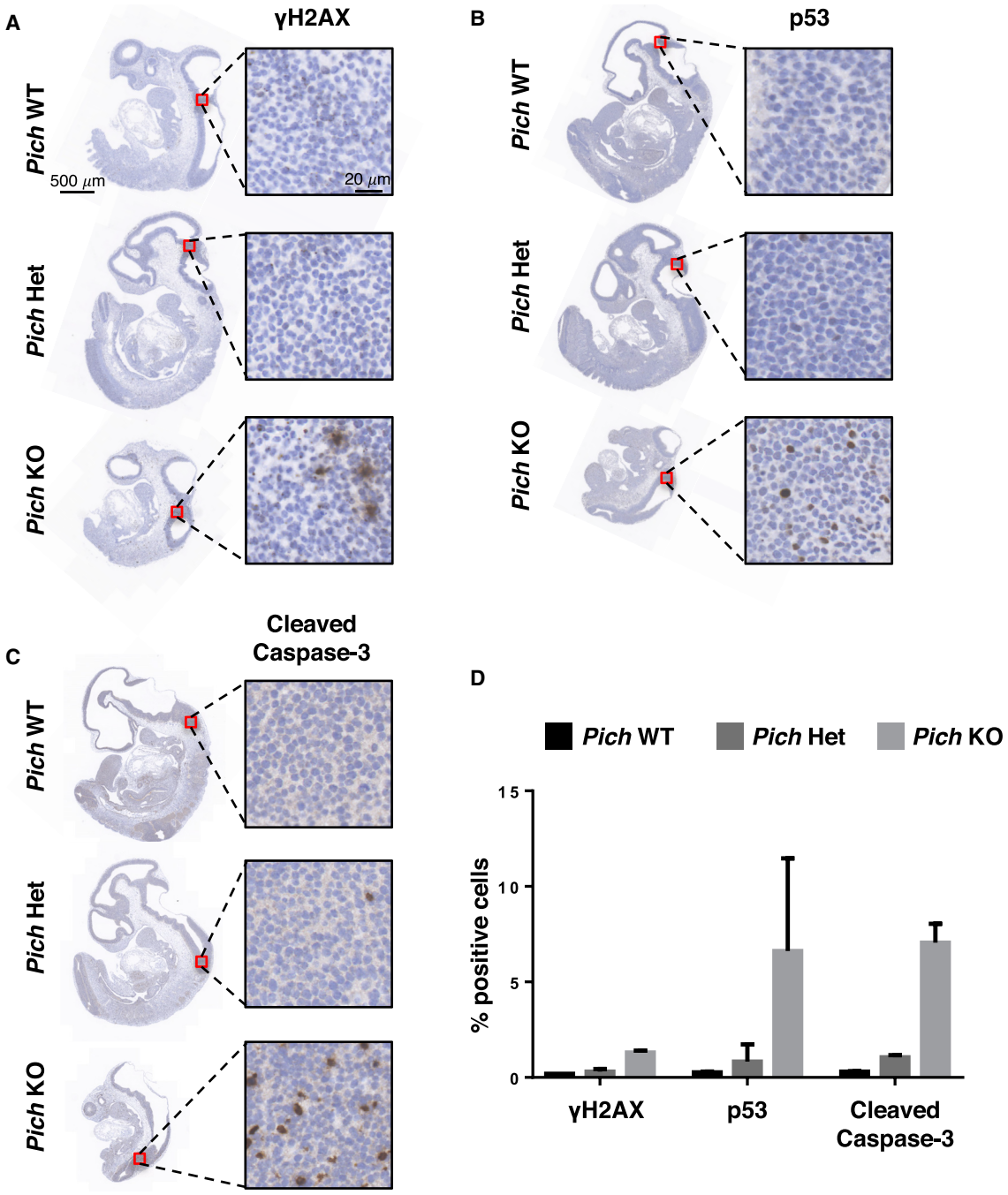

Figure 2. *Pich* KO Embryos Show Increased DNA Damage and Apoptosis as Compared to WT and Heterozygous Embryos

(A–C) Immunohistochemical staining of WT, *Pich* heterozygous (Het), and *Pich* KO embryos for γH2AX (A), p53 (B), and cleaved caspase-3 (C) at 10.5 DPC. (D) Quantification of the number of positive cells for γH2AX, p53, and cleaved caspase-3 in the brains of WT, *Pich* Het, and *Pich* KO 10.5 DPC embryos. Data shown correspond to four to six fields per embryo, counting at least 200 cells per field. For γH2AX, one WT embryo, two *Pich* Het, and two *Pich* KO embryos were assessed. For p53 and cleaved caspase-3, two WT, three *Pich* Het, and three *Pich* KO embryos were assessed.
Error bars indicate SD. See also Figures S1, S2, and S3.

tumorigenesis, which is another scenario of intense cell proliferation. We used the Xena browser (https://xena.ucsc.edu) and The Cancer Genome Atlas (TCGA) Pan-Cancer (PANCAN) dataset to analyze a potential correlation between PICH expression levels and the presence of mutations in TP53 and RB1, two of the tumor suppressor genes involved in cell-cycle regulation that are most frequently mutated in human cancers. Only truncating mutations (frameshift deletion or insertions and nonsense

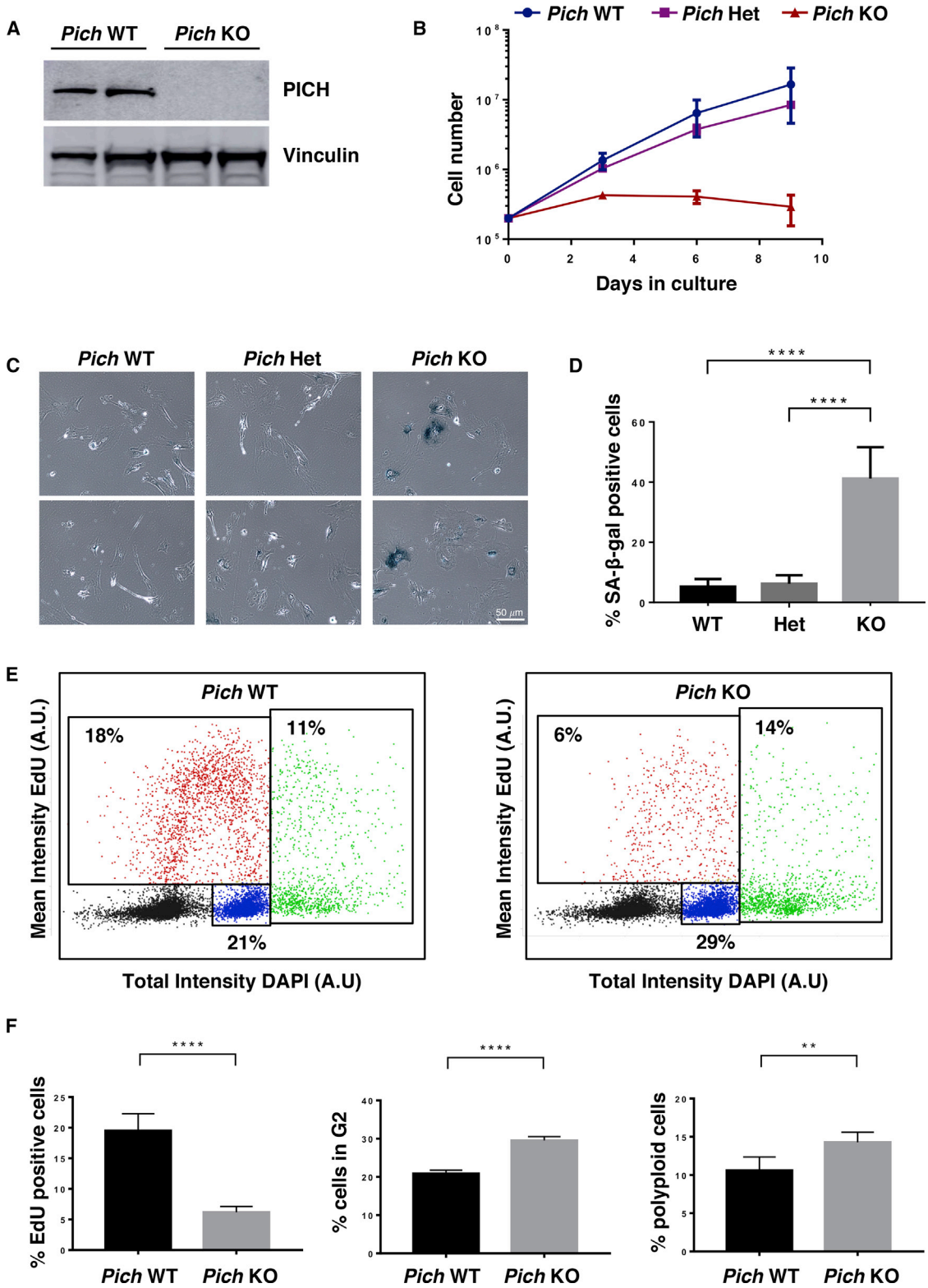

Figure 3. Characterization of *Pich* KO MEFs

(A) Western blotting confirming the absence of PICH protein in extracts from two *Pich* KO MEF cell lines as compared to WT MEF cell lines. Vinculin was used as the loading control.

(legend continued on next page)

mutations) were analyzed to disregard the potential gain of function mutations. PICH expression was significantly higher in cancer patient samples with truncating mutations in TP53 or in RB1 as compared to other samples without mutations in either of these genes (Figures S7A–S7D). Kaplan-Meier analysis showed that low PICH expression correlated with a better overall survival in cancer patients (Figure S7E). In addition, cancer type-specific survival was analyzed using the Kaplan-Meier Plotter tool (kmplot.com) (Győrffy et al., 2010), showing that lower PICH expression correlates with better overall survival in breast and lung cancer patients (Figures S7F and S7G).

PICH Is Required for RAS/E1A-Induced MEF Transformation and Growth

To investigate the requirement for PICH in cellular transformation *in vitro*, we performed classical MEF transformation assays by transducing *Pich* KO and WT MEFs with RAS^{V12}/E1A constructs. This transformation assay combines Ras activation and the effect of the viral oncoprotein E1A, which overrides the G1/S checkpoint by sequestering RB1 protein (Bandara and La Thangue, 1991). We found that *Pich* KO MEFs were not able to form colonies following the expression of these proteins (Figures 4D, 4E, and S4D), indicating that RAS^{V12}/E1A transformation is insufficient to override the proliferative defects of *Pich* KO primary MEFs. *Pich* Het MEFs were also refractory to transformation, giving rise to a fewer number of colonies as compared to WT MEFs (Figures 4D, 4E, and S4D), despite the fact that primary *Pich* Het MEFs were only slightly affected in terms of proliferation as compared to WT counterparts (Figure 3B). These *in vitro* data, together with our *in silico* analyses, suggest that PICH activity is important to sustain the proliferation of certain types of transformed or cancerous cells.

DISCUSSION

In this study, we report a PICH-deficient mouse model, which has allowed us to investigate the role of PICH during normal mammalian development. That *Pich* is located on the X chromosome and has an unusual, two-exon gene structure (with a short exon 1 and a long exon 2) have probably limited the generation of genetic models in the past.

Our results reveal that PICH is essential for embryonic development. *Pich* KO embryos exhibit genome instability that leads to generalized apoptosis, developmental arrest, and embryonic lethality. This genome instability is observed throughout the entire embryo. Thus, we believe that PICH function is important at the cellular level and particularly during embryonic development, when the rate of cell proliferation is very high. The penetrance of the lethal phenotype in the embryos is variable, with some KO embryos reaching day 13.5 (albeit with evidence of extensive cell death). A similar variability has been reported for other models that accumulate genomic instability, such as the *Atr-Seckel* (Murga et al., 2009) or *Brca1-Δ11* models (Xu et al., 2001). We believe that this variability likely reflects a stochastic degree of DNA damage accumulation and repair.

Pich Het females also exhibited a variable phenotype, ranging from perinatal lethality to the absence of any obvious defects. In principle, these Het females should be mosaic for *Pich* expression due to the random inactivation of one of the X chromosomes in female cells. However, and similar to several X-linked disorders, a bias in X chromosome inactivation (i.e., preferentially targeting the KO allele) could occur. We have analyzed PICH expression in four *Pich* Het embryos, observing a mosaic pattern that is compatible with random inactivation (Figures 1D and S1D). However, we cannot rule out an incomplete silencing of the WT *Pich* gene on the inactivated X chromosome, an observation that has been reported for *Pich* in mESCs (Marks et al., 2015). Further research will be required to understand the degree of *Pich* inactivation in adult mice and to investigate whether *Pich* Het females develop any age-associated phenotypes due to a progressive accumulation of DNA damage.

We observed a stabilization of p53 in *Pich* KO embryos, which is likely a consequence of the chronic activation of a DDR. In some mouse models with genomic instability, the activation of p53-dependent apoptosis and senescence programs accounts for the lethality observed during embryonic development (Frank et al., 2000; Xu et al., 2001). However, the inactivation of *Trp53* did not rescue the lethality caused by PICH deficiency. We believe that the extensive genomic alterations accumulated during the first 12 days of embryonic development in *Pich* KO embryos are incompatible with viability. Furthermore, this is most likely attributable to deleterious genome alterations rather than to chronic DDR activation and the subsequent p53-induced apoptosis.

We investigated the genetic interaction between *Pich* and *Trp53* in further detail and did not observe a significant rescue or potentiation of the phenotype of *Pich* KO embryos at 10.5 DPC in the absence of *Trp53*.

Of particular interest, we found that *Pich* Het females were born at a much-reduced frequency than expected in a *Tpr53* null background (only one was found of seven expected), suggesting that a partial synthetic lethal interaction between these genes may actually occur in a scenario with reduced levels of PICH. Consistent with this, we have found that *PICH* expression is significantly higher in cancer patient samples containing *TP53*

(B) Cell proliferation curve of WT, *Pich* Het, and *Pich* KO primary MEFs derived from 11.5 DPC littermate embryos. *Pich* KO MEFs proliferated at a lower rate than WT and *Pich* Het MEFs from passage one and stopped proliferating after four passages. Data represent means and SDs from two different cell lines per genotype, two replicates per cell line.
(C) Senescence-associated beta-galactosidase (SA-β-gal) staining of WT, *Pich* Het, and *Pich* KO MEFs.
(D) Quantification of the number of SA-β-gal^+ cells. Means and SDs were calculated from at least five fields per cell line and two cell lines per genotype.
(E) DNA replication rate and cell-cycle profile of WT and *Pich* KO MEFs determined by high-content microscopy. S-phase cells are shown in red, G2 cells in blue, and polyploid cells in green.
(F) Quantification of DNA replication rate (percentages of EdU incorporating cells) and percentages of G2 cells and polyploid cells from the cellular profiles shown in (E). Data shown correspond to means and SDs from two WT and two *Pich* KO MEF lines analyzed in technical triplicates.
$^{**}p \leq 0.01$; $^{****}p \leq 0.0001$.
See also Figure S4.

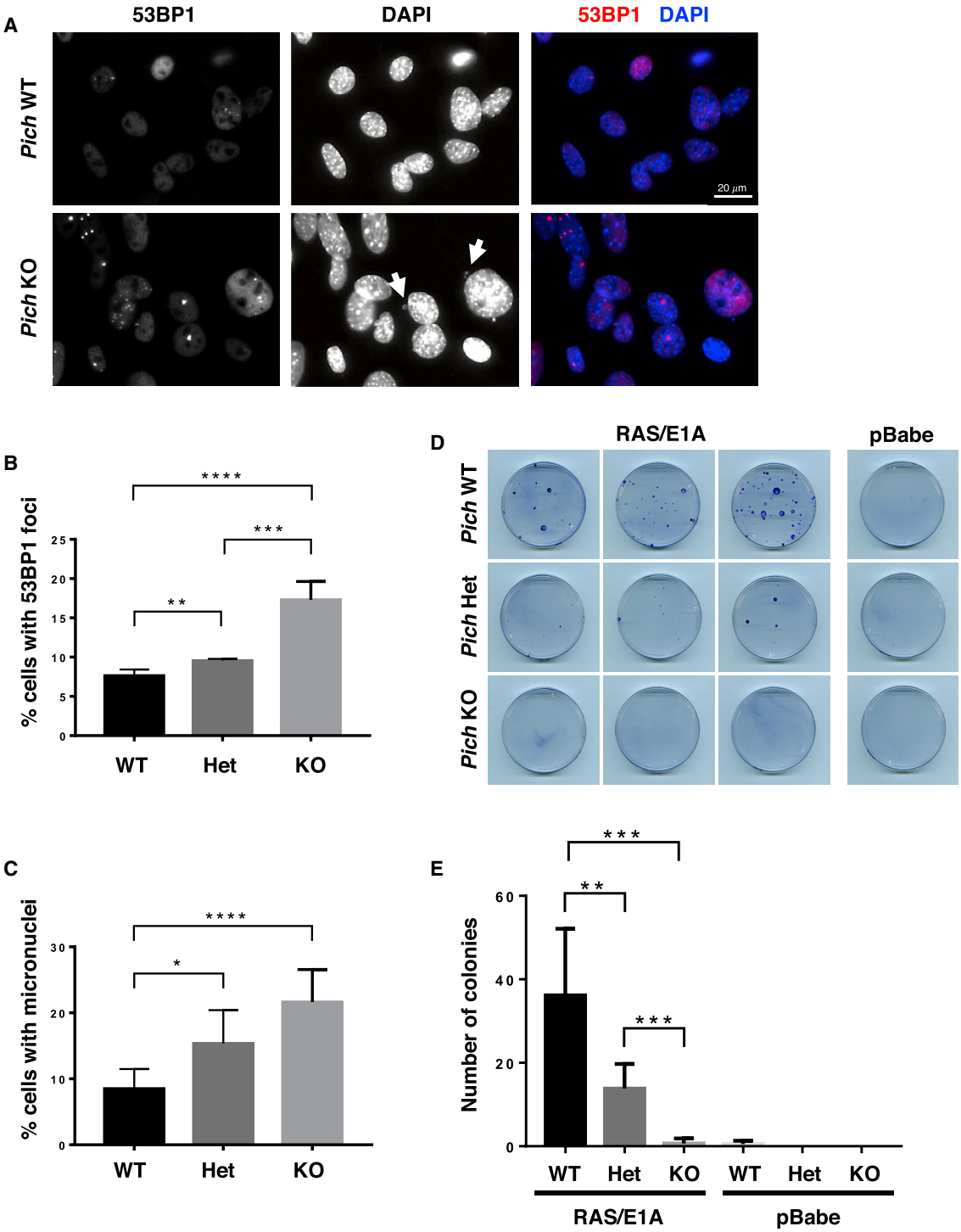

Figure 4. Genomic Instability and RAS^{V12}/E1A Transformation in *Pich* KO MEFs

(A) Representative images of immunofluorescence staining for 53BP1 in WT and *Pich* KO MEFs at early passages. Arrows indicate micronuclei, the number of which is increased in *Pich* KO MEFs.

(B) Quantification of cells with 53BP1 foci by high-content microscopy. Data correspond to three WT, one *Pich* Het, and two *Pich* KO MEF cell lines. Three wells were counted per cell line, with >1,000 cells for each three wells combined. Means and SDs are indicated.

(C) Quantification of cells with micronuclei. Images were acquired by an automated microscope and micronuclei were manually scored by two independent researchers. Data correspond to technical triplicates of three WT, one *Pich* Het, and two *Pich* KO MEF cell lines, counting three wells per cell line and at least 500 cells per sample. Means and SDs are indicated.

(legend continued on next page)

Table 3. Genotypes of Pups from *Pich*$^{+/-}$;*Trp53*$^{+/-}$ Females and *Trp53*$^{+/-}$ Males

Male Progeny						
	Pich^{+}			*Pich*$^{-}$		
	Trp53$^{+/+}$	*Trp53*$^{+/-}$	*Trp53*$^{-/-}$	*Trp53*$^{+/+}$	*Trp53*$^{+/-}$	*Trp53*$^{-/-}$
Observed	4	26	13	0	0	0
Expected	7	15	7	7	15	7
Female Progeny						
	Pich$^{+/+}$			*Pich*$^{+/-}$		
	Trp53$^{+/+}$	*Trp53*$^{+/-}$	*Trp53*$^{-/-}$	*Trp53*$^{+/+}$	*Trp53*$^{+/-}$	*Trp53*$^{-/-}$
Observed	10	23	8	11	21	1
Expected	7	15	7	7	15	7

See also Table S1 and Figures S5, S6, and S7.

truncating mutations as compared to samples without mutations in *TP53* (Figures S7A and S7B). This correlation is compatible with the idea that higher *PICH* expression may be required to sustain growth in tumors that have lost *TP53*. Further experimental research will be required to understand the functional relevance of these correlations. We believe that the *Pich* Het mESC is a relevant model for this purpose, particularly using cell differentiation protocols that promote X chromosome inactivation. In addition, our *in silico* analyses revealed that lower *PICH* expression correlated with an overall better survival across a wide range of cancer patient samples (TCGA Pan-Cancer dataset).

In line with the above, we observed that PICH is essential to sustain proliferation in transformed MEFs. In our studies, the use of an Ras^{V12}/E1A transformation assay combines Ras pathway activation with the expression of the viral oncoprotein E1A, which suppresses the G1/S checkpoint by sequestering RB1. We have also observed a correlation between high *PICH* expression levels and the presence of *RB1* mutations in human cancer samples. One plausible explanation for these correlations is that PICH activity is important for tumors with altered cell-cycle checkpoints caused by mutations in tumor suppressor genes such as *TP53* and *RB1*. Recent data derived from the use of siRNAs and shRNAs against PICH in breast and kidney cancer cell lines also support the idea that PICH is important for the proliferation of cancerous cells (Pu et al., 2017). Our findings are consistent with PICH being of critical importance for intense bouts of cell proliferation such as those during embryonic development and cancer. We believe that these findings open new avenues to investigate whether a strategy based on targeting PICH could provide a potential benefit for cancer patients.

EXPERIMENTAL PROCEDURES

Mouse Model Generation

The targeting construct for the *Pich (Ercc6l)* gene was generated by Gene Bridges (Heidelberg, Germany). It was linearized and incorporated into mESCs by targeted homologous recombination in collaboration with the Core Facility for Transgenic Mice at the University of Copenhagen. ESC clones containing the *Pich*$^{lox(neo)}$ allele were identified by PCR using primers *Pich*_F1 and *Pich* _R1 (Figures 1A, S1A, and S1B; see also sequences below). The expression of the allele was confirmed by RT-PCR (Albers et al., 2017) using primers *Pich*_F3 and *Pich* _R3 (data not shown; see also primers below). *Pich*$^{lox(neo)}$ ESCs were injected in mouse morulae, which were then transferred to pseudo-pregnant female mice to generate chimeras. The chimeras were then crossed with FLP-transgenic females (JAX strain 003800, Jackson Laboratory) (Rodríguez et al., 2000) and produced *Pich*$^{+/lox}$ female progeny. We generated *Pich*$^{+/-}$ females by crossing *Pich*$^{+/lox}$ females with UQ-CMV-Cre males (JAX strain 006054) (Schwenk et al., 1995). The *Pich* cKO strain has a mixed 129S2;C57BL/6N background. The *Trp53* KO strain has been described previously (JAX strain 002101) (Jacks et al., 1994). Mice were housed at the animal facility of the Department of Experimental Medicine at the University of Copenhagen and the research was monitored by the Institutional Animal Care and Use Committee. All of the mouse work was performed in compliance with Danish and European regulations.

Mouse Genotyping

Mice were genotyped using three primers—two surrounding the loxP site in exon 2 of the *Ercc6l* gene, *Pich*_F1 (5′-CTATGCCTGATCCTCCCCAG-3′) and *Pich*_R1 (5′-GCTAACAGACAAAATGGCCCT-3′), and one upstream of exon 1, *Pich*_F2 (5′-AAAGCCCAACTACAGTGTGG-3′) (Figure 1A). A 390-bp WT fragment and a 495-bp *Pich*$^{Lox(neo)}$ fragment were amplified using primers *Pich* _F1 and *Pich* _R1. The *Pich* KO allele was amplified by the *Pich* _R1 and *Pich* _F2 primer and generated a 220-bp fragment. RT-PCR was performed using primers *Pich*_F3 (5′-GTCTCCTTTCCTGGGCTCTC-3′′) and *Pich*_R3 (5′-AGGCTACAAGTGCCCAAGAA-3′).

Other primers used for genotyping were *Cre* (gCre5: 5′-TGGTTTCCCGCA GAACCTGAAG-3′ and gCre3: 5′-GAGCCTGTTTTGCACGTTCACC-3′), *Flippase* (FLP_F: 5′-CCCATTCCATGCGGGGTATCG-3′ and FLP_R: 5′-GCAT CTGGGAGATCACTGAG-3′), *Trp53* WT allele (KM057: 5′-GTGTTTCATTAG TTCCCCACCTTGAC-3′ and KM058: 5′-ATGGGAGGCTGCCAGTCCTAA CCC-3′), and *Trp53* KO allele (KM053: 5′-GTGGGAGGGACAAAAGTTC GAGGCC-3′ and KM054: 5′-TTTACGGAGCCCTGGCGCTCGATG-T-3′).

Embryo Characterization

Female mice were sacrificed between 10.5 and 13.5 DPC and embryos were kept in PBS and dissected. Yolk sac DNA was used for genotyping. Embryos were genotyped using the *Pich*_F1, *Pich*_F2, and *Pich*_R1 primers described in Mouse Genotyping. Embryo gender was determined by genomic PCR of

(D) RAS^{V12}/E1A transformation assay of WT, *Pich* Het, and *Pich* KO MEF cell lines with pBabe-Ras/E1A vector (left) and empty pBabe vector as control (right). Colony formation after seeding infected cells at low density and staining 2 weeks later.
(E) Quantification of the number of colonies in (D) and Figure S4D. Means and SDs were calculated from three (Ras/E1A) or two (pBabe) technical replicates and two MEF lines per genotype.
*p ≤ 0.05; **p ≤ 0.01; ***p ≤ 0.001; ****p ≤ 0.0001.
See also Figure S4.

Xist and *SRY* using the following primers: Xist_F (5′-GCTTTGTTTCAGTT TCTCTGG-3′), Xist_R (5′-ATTCTGGACCTATTGGGA-3′), SRY_F (5′-GCATT TATGGTGTGGTCC-3′), and SRY_R (5′-CCAGTCTTGCCTGTATGTGA-3′). Images were taken with an Olympus SC50 camera (Olympus) and a Leica M125 stereomicroscope (Leica Microsystems) before embryo fixation.

Embryos at 10.5 DPC were obtained by *in vitro* fertilization of oocytes from superovulated *Pich*$^{+/-}$;*Trp53*$^{+/-}$ females with sperm from *Trp53*$^{+/-}$ males and transferred to pseudopregnant recipient mothers. These procedures were performed following CARD/Infrafrontier protocols (https://www.infrafrontier.eu/knowledgebase/protocols/cryopreservation-protocols).

IHC

The IHC analyses were performed in collaboration with the Histopathology Core Unit at the Spanish National Cancer Research Centre (CNIO, Madrid, Spain). Mouse embryos were fixed in 4% neutral buffered formalin (Sigma-Aldrich), paraffin embedded, and processed according to standard procedures. For different staining methods, slides were deparaffinized in xylene and samples were rehydrated through graded concentrations of ethanol in water. Consecutive 3-μm sections were stained with H&E, and for IHC, an automated immunostaining platform was used (Ventana Discovery XT, Roche Diagnostics, or Autostainer Link, Dako). Antigen retrieval was performed with high or low (CC1m or RibCC, Roche; PICH, Dako) pH buffer, depending on the primary antibody, and endogenous peroxidase was blocked using 3% hydrogen peroxide. The primary antibodies used were γH2AX (JBV301; 1/25,000; MilliporeSigma, 05-636), p53 (POE316; 1/100; Monoclonal Core Unit CNIO, AM [POE316]), cleaved caspase-3 (1/750; Cell Signaling Technology, 9661) and PICH (D4G8; 1/50; Cell Signaling Technology, 8886). IHC reaction was developed using 3,3′-diaminobenzidine tetrahydrochloride (DAB) (Chromomap DAB, Ventana, Roche; DAB+ Chromogen System, Dako). Nuclei were counterstained with Carazzi's hematoxylin. Images were acquired using a slide scanner (AxioScan Z1, Zeiss).

MEF Generation and Cell Culture

MEFs were obtained from 11.5 or 12.5 DPC embryos following standard procedures and cultured in DMEM (GIBCO) supplemented with 15% fetal bovine serum (FBS) and 1% penicillin-streptomycin. For the proliferation assay, 200,000 (Figures 3B and S4B) or 100,000 cells (Figure S4A) were plated in a well of a 6-well plate. Every 3 to 4 days, cells were counted and replated at a density of 200,000 cells/well (Figures 3B and S4B) or 100,000 cells/well (Figure S4A). MEFs were stained at passage seven for senescence-associated beta-galactosidase (SA-β-gal) using the Senescence Cells Histochemical Staining Kit (Sigma-Aldrich CS0030).

Immunofluorescence and High-Content Microscopy

MEFs and mESCs were grown in μCLEAR 96-well plates (Greiner Bio-One) for 2 days, before fixation in 4% paraformaldehyde (PFA) and stained according to standard procedures. The primary antibodies used were 53BP1 (Novus Biologicals 100-304A2) and γH2AX (MilliporeSigma, 05-636). The DNA replication rate was determined by EdU incorporation using Click-iT technology following the manufacturer's instructions (Life Technologies). Images were acquired with the ScanR acquisition software (Olympus) controlling a motorized Olympus IX-81 wide-field microscope and analyzed and quantified with the ScanR Analysis software.

Western Blotting

MEFs and mESCs were lysed with radioimmunoprecipitation assay (RIPA) buffer (Sigma-Aldrich) containing phosphatase (Sigma-Aldrich) and protease inhibitor cocktails (Roche). Membranes were blocked in 5% BSA in PBS with Tween 20 (PBS-T) for 1 hr before primary antibody incubation for PICH (1/1,000, Cell Signaling Technology, 8886), p53 (1/1,000, Santa Cruz Laboratories sc-393031) or vinculin (1/1,000, Sigma-Aldrich V9264). The secondary antibody for PICH was goat anti-rabbit immunoglobulin G (IgG) (1/10,000, Sigma-Aldrich A6667); for p53 and vinculin, it was goat anti-mouse IgG (1/10,000, Sigma-Aldrich A4416). Images were acquired on an Amersham Imager 600 (GE Healthcare Life Sciences).

MEF Transformation Assay

Early passage MEFs were transduced with a pBabe-RAS^{V12}/E1A retroviral vector (gift from M. Barbacid, CNIO, Madrid, Spain) or a pBabe empty vector according to standard procedures. Two days after transduction, cells were selected with 2 μg/mL puromycin for 2 days. After selection, 10,000 cells were seeded on 10-cm Petri dishes and stained with crystal violet after 2 weeks.

mESC Transduction

mESCs were obtained from *in vitro* fertilization of *Pich*$^{+/-}$ oocytes with WT spermatocytes, performed at the Core Facility for Transgenic Mice at the University of Copenhagen. For the transduction with retroviral vectors encoding control and p53 shRNA previously validated (Murga et al., 2009), 300,000 cells were transduced in suspension with 1 mL retroviral supernatant and 1 μg/mL polybrene. After selection with 1 μg/mL puromycin, cells were seeded on gelatin-coated μCLEAR 96-well plates for immunofluorescence and high-content microscopy (see above).

Statistical Analysis

Statistical significance was determined with the unpaired t test in GraphPad Prism 7. p values are indicated above the graphs: *$p \leq 0.05$; **$p \leq 0.01$; ***$p \leq 0.001$; ****$p \leq 0.0001$.

SUPPLEMENTAL INFORMATION

Supplemental Information includes seven figures and one table and can be found with this article online at https://doi.org/10.1016/j.celrep.2018.08.071.

ACKNOWLEDGMENTS

This work was funded by the Danish National Research Foundation (DNRF115), the Danish Council for Independent Research (Sapere Aude, DFF-Starting Grant 2014, DFF-4004-00185), the Danish Cancer Society (KBVU-2014_R09-A6031 and KBVU-2017_R167-A11063), the European Research Council (ERC-2015-STG-679068), and the Lundbeck Foundation (R218-2016-415). We thank Toyota Fonden and Læge Sofus Carl Emil Friis og hustru Olga Doris Fonden for funding the acquisition of the high-content microscope used in this study. We thank Dr. Hocine Mankouri and Dr. Berta L. Sanchez-Laorden for critical reading and editing of the manuscript. We thank Maria Gómez and Zaira Vega from the CNIO Histopathology Core Unit for technical support. We also thank the Core Facility for Transgenic Mice and the Department of Experimental Medicine at the University of Copenhagen.

AUTHOR CONTRIBUTIONS

E.A. and M.S. designed, performed, and analyzed most of the experiments. D.P.-M. helped with the high-content data analyses. A.A. provided important technical help for the cell culture-related experiments. I.D.H. and A.H.B. provided critical input and advice during the development of the project. P.G. performed the pathology work. J.M.-G. assisted in the mouse model generation and derived mESCs. A.J.L.-C. conceived, designed, and supervised the study. A.J.L.-C., M.S., and E.A. wrote the manuscript. All of the authors read, edited, and commented on the manuscript.

DECLARATION OF INTERESTS

The authors declare no competing interests.

Received: November 10, 2017
Revised: July 18, 2018
Accepted: August 23, 2018
Published: September 18, 2018

REFERENCES

Albers, E., Sbroggiò, M., Martin-Gonzalez, J., Avram, A., Munk, S., and Lopez-Contreras, A.J. (2017). A simple DNA recombination screening method by RT-PCR as an alternative to Southern blot. Transgenic Res. *26*, 429–434.

Bandara, L.R., and La Thangue, N.B. (1991). Adenovirus E1a prevents the retinoblastoma gene product from complexing with a cellular transcription factor. Nature *351*, 494–497.

Baumann, C., Körner, R., Hofmann, K., and Nigg, E.A. (2007). PICH, a centromere-associated SNF2 family ATPase, is regulated by Plk1 and required for the spindle checkpoint. Cell *128*, 101–114.

Biebricher, A., Hirano, S., Enzlin, J.H., Wiechens, N., Streicher, W.W., Huttner, D., Wang, L.H., Nigg, E.A., Owen-Hughes, T., Liu, Y., et al. (2013). PICH: a DNA translocase specially adapted for processing anaphase bridge DNA. Mol. Cell *51*, 691–701.

Chan, K.L., North, P.S., and Hickson, I.D. (2007). BLM is required for faithful chromosome segregation and its localization defines a class of ultrafine anaphase bridges. EMBO J. *26*, 3397–3409.

Frank, K.M., Sharpless, N.E., Gao, Y., Sekiguchi, J.M., Ferguson, D.O., Zhu, C., Manis, J.P., Horner, J., DePinho, R.A., and Alt, F.W. (2000). DNA ligase IV deficiency in mice leads to defective neurogenesis and embryonic lethality via the p53 pathway. Mol. Cell *5*, 993–1002.

Győrffy, B., Lanczky, A., Eklund, A.C., Denkert, C., Budczies, J., Li, Q., and Szallasi, Z. (2010). An online survival analysis tool to rapidly assess the effect of 22,277 genes on breast cancer prognosis using microarray data of 1,809 patients. Breast Cancer Res. Treat. *123*, 725–731.

Haupt, S., Berger, M., Goldberg, Z., and Haupt, Y. (2003). Apoptosis - the p53 network. J. Cell Sci. *116*, 4077–4085.

Hengeveld, R.C., de Boer, H.R., Schoonen, P.M., de Vries, E.G., Lens, S.M., and van Vugt, M.A. (2015). Rif1 is required for resolution of ultrafine DNA bridges in anaphase to ensure genomic stability. Dev. Cell *34*, 466–474.

Hübner, N.C., Wang, L.H., Kaulich, M., Descombes, P., Poser, I., and Nigg, E.A. (2010). Re-examination of siRNA specificity questions role of PICH and Tao1 in the spindle checkpoint and identifies Mad2 as a sensitive target for small RNAs. Chromosoma *119*, 149–165.

Itahana, K., Dimri, G., and Campisi, J. (2001). Regulation of cellular senescence by p53. Eur. J. Biochem. *268*, 2784–2791.

Jacks, T., Remington, L., Williams, B.O., Schmitt, E.M., Halachmi, S., Bronson, R.T., and Weinberg, R.A. (1994). Tumor spectrum analysis in p53-mutant mice. Curr. Biol. *4*, 1–7.

Mankouri, H.W., Huttner, D., and Hickson, I.D. (2013). How unfinished business from S-phase affects mitosis and beyond. EMBO J. *32*, 2661–2671.

Marks, H., Kerstens, H.H., Barakat, T.S., Splinter, E., Dirks, R.A., van Mierlo, G., Joshi, O., Wang, S.Y., Babak, T., Albers, C.A., et al. (2015). Dynamics of gene silencing during X inactivation using allele-specific RNA-seq. Genome Biol. *16*, 149.

Murga, M., Bunting, S., Montaña, M.F., Soria, R., Mulero, F., Cañamero, M., Lee, Y., McKinnon, P.J., Nussenzweig, A., and Fernandez-Capetillo, O. (2009). A mouse model of ATR-Seckel shows embryonic replicative stress and accelerated aging. Nat. Genet. *41*, 891–898.

Nielsen, C.F., and Hickson, I.D. (2016). PICH promotes mitotic chromosome segregation: identification of a novel role in rDNA disjunction. Cell Cycle *15*, 2704–2711.

Nielsen, C.F., Huttner, D., Bizard, A.H., Hirano, S., Li, T.N., Palmai-Pallag, T., Bjerregaard, V.A., Liu, Y., Nigg, E.A., Wang, L.H., and Hickson, I.D. (2015). PICH promotes sister chromatid disjunction and co-operates with topoisomerase II in mitosis. Nat. Commun. *6*, 8962.

Pu, S.Y., Yu, Q., Wu, H., Jiang, J.J., Chen, X.Q., He, Y.H., and Kong, Q.P. (2017). ERCC6L, a DNA helicase, is involved in cell proliferation and associated with survival and progress in breast and kidney cancers. Oncotarget *8*, 42116–42124.

Rodríguez, C.I., Buchholz, F., Galloway, J., Sequerra, R., Kasper, J., Ayala, R., Stewart, A.F., and Dymecki, S.M. (2000). High-efficiency deleter mice show that FLPe is an alternative to Cre-loxP. Nat. Genet. *25*, 139–140.

Rouzeau, S., Cordelières, F.P., Buhagiar-Labarchède, G., Hurbain, I., Onclercq-Delic, R., Gemble, S., Magnaghi-Jaulin, L., Jaulin, C., and Amor-Guéret, M. (2012). Bloom's syndrome and PICH helicases cooperate with topoisomerase IIα in centromere disjunction before anaphase. PLoS One *7*, e33905.

Schwenk, F., Baron, U., and Rajewsky, K. (1995). A cre-transgenic mouse strain for the ubiquitous deletion of loxP-flanked gene segments including deletion in germ cells. Nucleic Acids Res. *23*, 5080–5081.

Xu, X., Qiao, W., Linke, S.P., Cao, L., Li, W.M., Furth, P.A., Harris, C.C., and Deng, C.X. (2001). Genetic interactions between tumor suppressors Brca1 and p53 in apoptosis, cell cycle and tumorigenesis. Nat. Genet. *28*, 266–271.